Supporting Information: A Comparison of Coarse-Grained and Continuum Models for Membrane Bending in Lipid Bilayer Fusion Pores

[†]Jejoong Yoo, [†,¶]Meyer B. Jackson, [†,‡]Qiang Cui[1]

[†]*Graduate Program in Biophysics,*
[¶]*Department of Neuroscience,*
[‡]*Department of Chemistry and Theoretical Chemistry Institute,*
University of Wisconsin, Madison, 1101 University Avenue, Madison, WI 53706

December 27, 2012

[1]Correspondence should be sent to mbjackso@wisc.edu, cui@chem.wisc.edu.

Computation of average phosphate surfaces

We compute the phosphate surfaces in the $x-z$ plane by averaging phosphate positions in the last 100 ns of a simulation. Phosphate positions are recorded every 1,000 steps. Because the fusion pore axis migrates significantly in the $x-y$ plane in long simulations, we first determine the average position of the fusion pore axis by making a phosphate density map in the $x-y$ plane over the last 100 ns. Once the fusion pore axis is determined, we make a phosphate density map in the $x-z$ plane by averaging phosphate density over the azimuthal angle. Because fusion pore structures are symmetric with respect to the pore axis, the density map in the $x-z$ plane should be well defined when a simulation reaches equilibrium. Finally, we compute the average phosphate surface of each monolayer by averaging the monolayer density map.

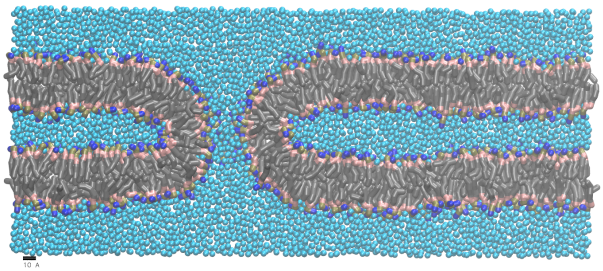

Figure S1: The fusion pore configuration of the CG-DPPC-R_b system with $R_b = 3.7$ nm at the end of the simulation shows the bilayer thinning at the pore center. A snapshot of a 1-nm slab parallel to the z-axis is shown here. Coarse-grained beads are colored by their types: hydrocarbon, gray; glycerol, pink; phosphate, tan; choline, blue; water, cyan.

Equilibration of lipid/water with the exchange hole protocol at the CG level

To demonstrate the equilibration process of curved membrane using the exchange hole scheme we carry out coarse-grained (MARTINI) simulations of a vesicle with a mixture of three different species: DPPC, DPPE, and LPC. For this purpose, we choose a vesicle because it is relatively easy to monitor quantitatively the number of lipid in each monolayer due to the spherical symmetry of a vesicle. We build the initial conformation by randomly changing certain numbers of DPPC to DPPE or LPC in a pre-equilibrated vesicle with 2621 DPPC molecules; the mixture vesicle contains 600 LPC, 600 DPPE, and 1421 DPPC molecules. We prepare three conformations with different initial distributions of lipids. For each of the conformations, we perform a simulation for about 1 μs with six exchange holes. We place the vesicle at origin, and the holes are made by defining three soft harmonic potentials (Eq. 1 in the main text) about x, y, and z axes. The simulation details and the parameters for the soft harmonic potentials are identical to those used for the coarse-grained simulations of the fusion pores. As shown in Fig.S2, the lipid distributions start to converge after about 500-600 ns, and the final distributions are close to those reported in the literature(6). Therefore, the exchange hole protocol appears effective for equilibrating lipid/water distributions.

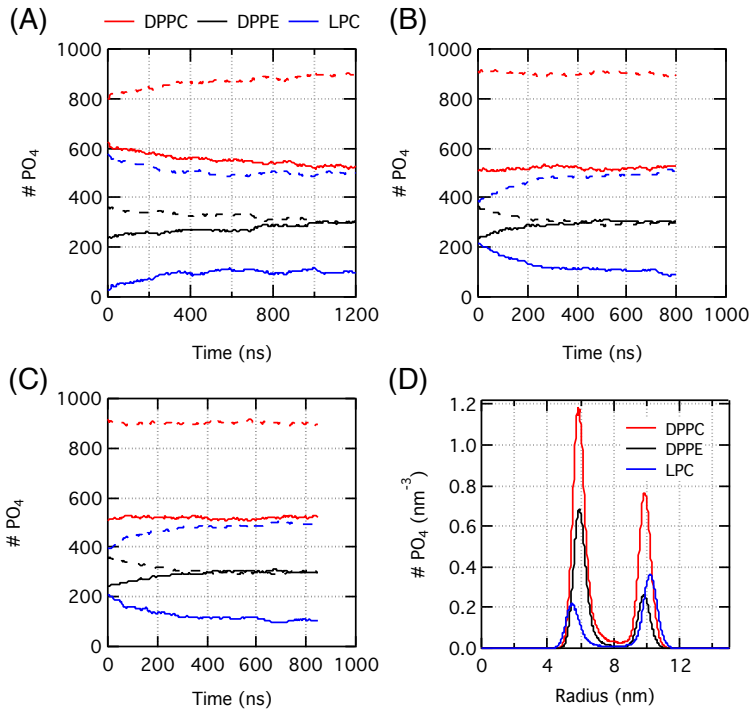

Figure S2: Coarse-grained simulations of vesicles. (A–C) show the number of each lipid species (DPPC, red; DPPE, black; LPC, blue) in the inner (in solid line) and outer (in dashed line) layers as a function of time from three simulations with random initial configurations. Note that the final lipid compositions in each layer are almost identical for three simulations, demonstrating the effectiveness of the exchange hole scheme we employed in this study. (D) shows the phosphate density plot of each species as a function of the distance from the center of vesicle at the end of simulation. Relatively high density of LPC and DPPE in the outer and inner layers, respectively, is consistent with the observations by Marrink et al. in their coarse-grained simulations of spontaneous vesicle formations (6).

Coarse-grained simulations with perturbed fusion pore

To test the hypothesis that the fusion pore undergoes slow structural relaxation, we perform three additional coarse-grained simulations (CG–DOPC–PERT1, 2, 3 in Table 1 of the main text), in which we start a simulation with a structural perturbation from the final snapshot of CG–DOPC. For CG–DOPC–PERT1, we extend the flat bilayer region by 20 nm in both the x and y dimensions. We build a double bilayer system with a given bilayer-bilayer separation (R_b), and after a short equilibration the central region of this double bilayer is replaced by the CG–DOPC system that contains the equilibrated fusion pore. For CG–DOPC–PERT2, we elongate the fusion pore of CG–DOPC along the z-axis by 4 nm; all molecules at $z > 0$ and $z < 0$ are shifted by 2 and -2 nm along the z-axis and the empty space with $|z| < 2$ nm is filled with a 4-nm segment ($|z| < 2$ nm) taken from the CG–DOPC system. For CG–DOPC–PERT3, we pressurize the regions confined by the asymptotic bilayers by doubling the number of water molecules; we duplicate the water beads in this region and then randomly translate all duplicated water beads by < 1 Å in all three directions. The three structurally perturbed configurations are energy-minimized for 5,000 steps, and then equilibrated with a short time step of 2 fs for a few nanoseconds to remove the instabilities of the systems caused by the structural perturbations. Then, we carry out long simulations ranging from 500 to 2,500 ns with a 40 fs time step.

As an example for the time scale of structural relaxation, we show the behavior of CG–DOPC–PERT2 in Fig.S3. The major redistribution of lipids has finished within 200 ns. Neverthelss, the three perturbations do not lead to the same fusion pore structure (see Fig.S4), indicating that the fusion pore undergoes a very slow conformational relaxation beyond the μs scale studied here.

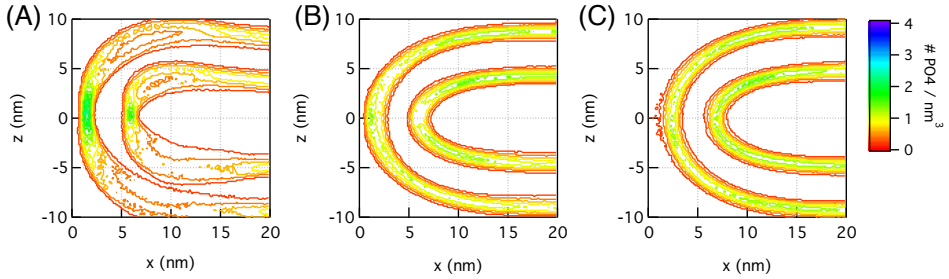

Figure S3: Changes in phosphate density map of the fusion pore system CG-DOPC-PERT2 during the 800 ns simulation. The density maps are computed using three time segments: 0-50 (A), 100-200 (B), and 700-800 ns (C). Note that the phosphate density map is rather broadly distributed in (A) due to asymmetry caused by the structural perturbation. However, the fusion pore structure recovers the symmetry within ∼200 ns.

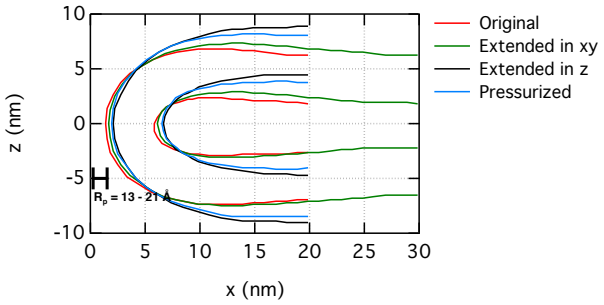

Figure S4: Average phosphate surfaces at the end of the CG–DOPC and CG–DOPC–PERT1, 2, 3 simulations. Note that fusion pore configurations do not converge to a unique shape after ∼300 ns, indicating that the fusion pore undergoes a very slow conformational relaxation.

Coarse-grained simulations with asymptotic planar restraints

As discussed in the Result section, the CG simulations might not reach equilibrium due to the slow relaxation of the lipids in regions far from the fusion pore. To explore how these 'asymptotic' regions impact the structure of the fusion pore, we set up simulations (CG–DOPC–R_b and CG–DPPC–R_b in Table 1 of the main text; results shown in Fig.S5) with the lipids in these regions subject to planar restraints. Specifically, we keep the outer monolayers flat at $r > 13$ nm by applying the following harmonic restraint,

$$V^{\text{plane}} = 0.5k(|z| - z_0)^2 + 0.5k\Theta(13\text{ nm} - r)(r - 13\text{ nm})^2 \quad (1)$$

to 500 phosphate beads chosen in each of the upper and lower outer monolayers (red lines in Fig.2 of the main text), where z_0 is the equilibrium position of those chosen phosphate groups and k equals 100 kJ/mol·nm^2. The restrained phosphate groups account for ∼20 % of the total phosphate groups in the outer monolayers at $r > 13$ nm. The restrained phosphate groups are free to move in the $x-y$ directions so that an optimal lipid density is maintained, and the restraints do not directly affect the fusion pore structure because the restrained phosphate groups are separated from the fusion pore by at least 13 nm. Because the equilibrium distance between two phosphate surfaces of a DPPC and DOPC bilayer is about 4.2 and 4.4 nm, respectively, we restrain R_b to $z_0 + 2.1$ (DPPC) and $z_0 + 2.2$ nm (DOPC). For each R_b parameter, we run simulations for ∼300 ns.

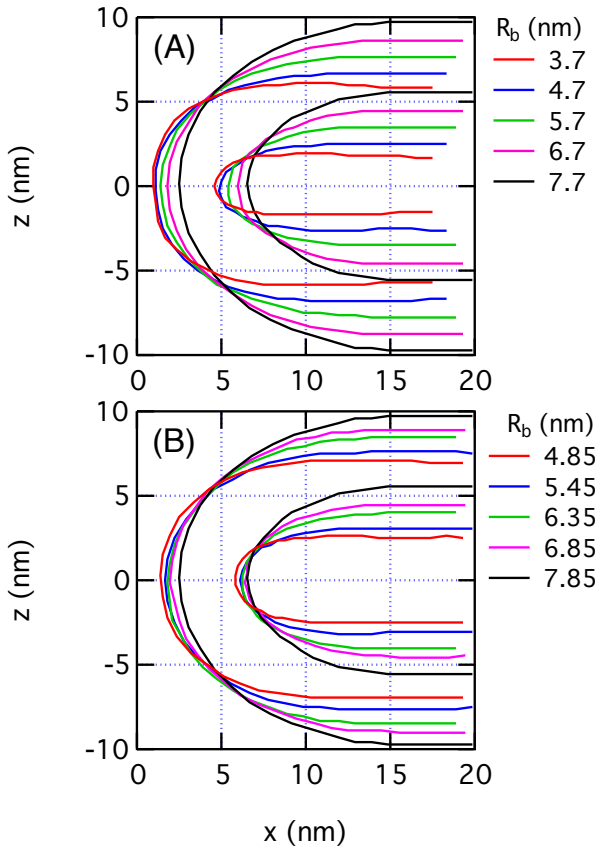

Figure S5: Average phosphate surfaces of CG–DPPC–R_b (A) and CG–DOPC–R_b (B) simulations with planar restraints for outer monolayers at $r > 13$ nm (Eq. 1) with R_b ranging from about 3 to 8 nm.

Comparison of atomistic and CG fusion pores

We also carry out brief comparison between atomistic and CG simulations for the fusion pore structure. As discussed above, there are slow relaxations on the microsecond and beyond, thus it's not practical to carry out entirely independent atomistic simulations for the fusion pore. Instead, we start with the fusion pore predicted from the CG simulations and examine its structural stability at the atomistic level at the hundred nanosecond time scale. If there are major differences between the CG and atomistic predictions for the fusion pore structure, we believe they would have been observed at this time scale.

Table 1: Summary of the simulation setups for smaller systems

	Composition		Box dimension	Simul. time	Exchange	Planar
System	Lipid	Water	(nm^3)	(ns)	holes	restraints
CG–DOPC–SML	1,665	20,400	$16 \times 16 \times 14$	400	No	No
AA–DOPC–SML	1,665	81,600	$16 \times 16 \times 14$	100	No	No

To simulate the fusion pore at the atomistic level, a smaller system (see Table S1) is prepared with the following procedure. First, we make a smaller CG fusion pore of about 16 nm $\times$ 16 nm $\times$ 14 nm (CG–DOPC–SML) by deleting molecules with $|x|, |y| > 8$ nm or $|z| > 7$ nm in the pre-equilibrated CG–DOPC system; the CG–DOPC–SML system includes 1,665 DOPC and 20,400 CG water beads. The CG–DOPC–SML system is simulated for 200 ns. Then, we use the CHARMM package(1) for the CG to AA conversion. For the conversion of each lipid, we load a CG lipid from the pre-equilibrated fusion pore and an arbitrary all-atom lipid conformation into CHARMM. With the CG lipid fixed in space, we apply a harmonic restraint between a CG bead and the the center-of-mass of the corresponding group of atoms in the atomistic model (e.g., PO_4 bead in MARTINI and phosphate atoms). With a short minimization, we can successfully superimpose an all-atom lipid over a CG lipid. By repeating this procedure, we convert the entire fusion pore system into an atomistic representation. In a similar manner, a cluster of four water molecules replaces a CG water bead. This all-atom system contains 1,665 all-atom DOPC and 81,600 water molecules, and we label this system AA–DOPC–SML. For efficient calculations, we employ the united-atom lipid model by Berger et al. (2) in combination with the SPC water model (3). Due to the relatively small system size, we do not use the exchange holes.

For atomistic simulations we also use the semi-isotropic set up with constant temperature (323 K) and zero surface tension. A cut-off scheme of 10 Å is used for Lennard-Jones interactions and the particle mesh Ewald method for electrostatic interactions (4, 5). The integration time step is 2 fs. As summarized in Table 1 in the main text, the simulation time scale is $\sim$100 ns. At this time scale, the fusion pore does not undergo any major change (see Fig.S6), suggesting that the fusion pores at the AA and CG levels are very similar.

Fig. S7A and S7B show the phosphate number density maps of the CG–DOPC–SML and AA–DOPC–SML systems. Compared to the CG–DOPC system in Fig.4 of the main text, the phosphate density maps of the smaller systems show slightly thinner bands, indicating a more rigid structure for the smaller system. Because of the smaller system size and the lack of exchange holes in these simulations, the fusion pore structures in Fig. S7A,B seem slightly different from that in Fig.4 of the main text. Nevertheless, these simulations are sufficient to test the agreement between AA and CG models. Overall, Fig. S7A and S7B show a reasonable agreement, as shown more explicitly by a comparison of the average phosphate surfaces from CG–DOPC–SML and AA–DOPC–SML systems in Fig. S7C. This observation provides further support to the use of MARTINI to probe the structure of fusion pores. An interesting difference is that the AA pore at the center is thinner than

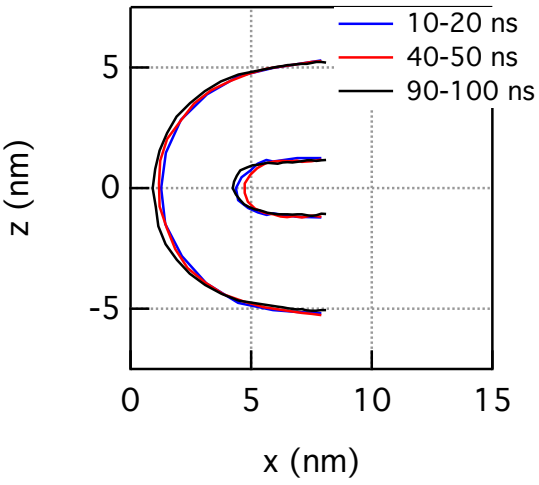

Figure S6: Changes in average phosphate surfaces as functions of time during the 100 ns simulation of AA-DOPC-SML system.

the CG pore; this likely reflects that in a region of extremely high curvature the lower resolution (thus the less degree of tail flexibility) of the CG model becomes less accurate.

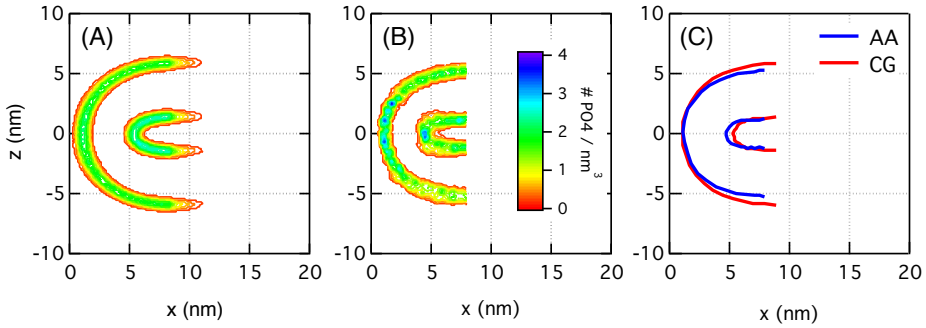

Figure S7: Phosphate density maps of the fusion pore from (A) CG–DOPC–SML (B) AA–DOPC–SML; compare those to the density map of the CG–DOPC simulation shown in Fig. 4 of the main text. (C) Comparison of the average phosphate surfaces from CG–DOPC–SML and AA–DOPC–SML simulations.

Continuum minimizations with different initial conditions

To better compare minimized structures at the continuum level with the results of CG simulations, we have explored multiple initial conditions for the continuum minimizations. As illustrated in Fig.S8A for DOPC and R_b = 5.75 nm, these initial conditions are very different in shape and energy. Nevertheless, minimizations starting with these initial guesses lead to largely similar final results with a narrow energy spread of 6 k_BT (Fig.S8B). The lowest energy solution is obtained when using the CG structure as the initial guess, again reflecting that the CG result is very close to an energetically favorable solution at the continuum level.

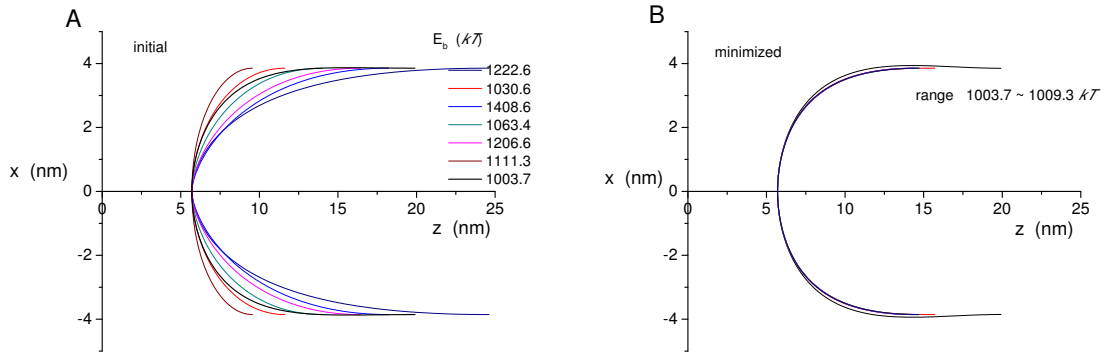

Figure S8: The impact of initial condition on the result of the continuum model for DOPC and R_b = 5.75 nm. (A) The shape contour of different initial guesses and their energies; (B) Minimized shape contours and the spread of their energies.

Results for DPPC from continuum analysis

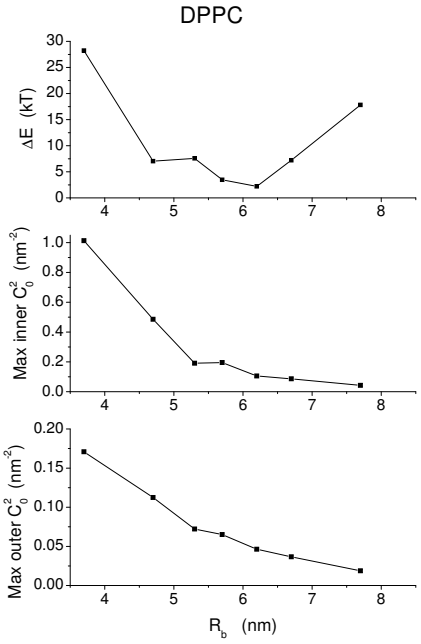

Figure S9: Top row: The energy reduction achieved by minimization of E_b is plotted versus R_b for DPPC. These plots show very low reductions in energy for intermediate values of R_b and somewhat larger reductions for larger and smaller values of R_b. The maximum square mean curvatures of the inner (middle row) and outer (bottom row) monolayers show sharp increases at low R_b and become very small for large R_b.

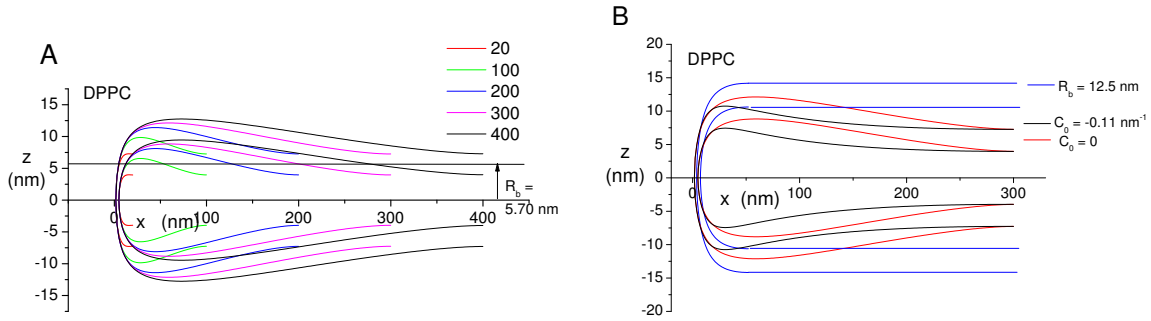

Figure S10: Continuum model fusion pores of DPPC bilayers of various sizes. Increasing the size allows for profound bowing during energy minimization. For the largest systems the maximal distance between the two fusing bilayers is roughly twice the limiting distance at large x.(B) Continuum model fusion pores reveal the effect of changing C_0 to zero and increasing R_b to about that seen at the height of bowing. Zero C_0 shifts the bowing to large x. Larger R_b values eliminate bowing.

References

1. Brooks, B. R., C. L. Brooks, III, A. D. Mackerell, L. Nilsson, R. J. Petrella, B. Roux, Y. Won, G. Archontis, C. Bartels, S. Boresch, A. Caflisch, L. Caves, Q. Cui, A. R. Dinner, M. Feig, S. Fischer, J. Gao, M. Hodoscek, W. Im, K. Kuczera, T. Lazaridis, J. Ma, V. Ovchinnikov, E. Paci, R. W. Pastor, C. B. Post, J. Z. Pu, M. Schaefer, B. Tidor, R. M. Venable, H. L. Woodcock, X. Wu, W. Yang, D. M. York, and M. Karplus, 2009. CHARMM: The Biomolecular Simulation Program. *J. Comp. Chem.* 30:1545–1614.

2. Berger, O., O. Edholm, and F. Jähnig, 1997. Molecular dynamics simulations of a fluid bilayer of dipalmitoylphosphatidylcholine at full hydration, constant pressure, and constant temperature. *Biophys. J.* 72:2002–13.

3. Berendsen, H. J. C., J. P. M. Postma, W. F. van Gunsteren, and J. Hermans, 1981. Intermolecular forces, Reidel, Dordrecht.

4. Darden, T., D. York, and L. Pedersen, 1993. Particle mesh Ewald: An N log(N) method for Ewald sums in large systems. *J. Chem. Phys.* 98:10089–10092.

5. Essmann, U., L. Perera, M. L. Berkowitz, T. Darden, H. Lee, and L. G. Pedersen, 1995. A smooth particle mesh Ewald method. *J. Chem. Phys.* 103:8577–8593.

6. Marrink, S. J., and A. E. Mark, 2003. Molecular dynamics simulation of the formation, structure, and dynamics of small phospholipid vesicles. *J. Am. Chem. Soc.* 125:15233–42.